ЖЭТФ, 2003, том 123, вып. 5, стр. 1082–1089

TIME REVERSAL SYMMETRY BREAKING IN CUPRATES INDUCED BY THE SPIRAL SPIN ORDER

M. Ya. Ovchinnikova*

Institute of Chemical Physics, Russian Academy of Sciences
117334, Moscow, Russia

Submitted 1 November 2002

We propose a new interpretation of the spontaneous time reversal symmetry breaking (TRSB) observed recently in a pseudogap state of cuprates (Kaminsky et al.). It is shown that the TRSB dichroism in ARPES signal may be related to the local spin spiral structures in the system. It may be caused by a spin–orbit interaction and by spin polarization of electrons at various sections of the Fermi surface in the spiral state. The angular dependence of the dichroism signal is studied in a schematic KKR approximation. Tests are proposed to check the existence of the local spiral spin structure and to distinguish it from the TRSB state with micro-currents constructed by Varma.

PACS: 71.10.Fd, 74.20.Rp, 74.20.-z

The nature of a pseudogap (PS) state of high-T_c cuprates in the underdoped (UD) region remains an intriguing problem [1, 2]. Using the angular-resolved photoemission (ARPES) with circularly polarized light (CPL), Kaminsky et al. [3] recently revealed a new property of the pseudogap state of UD $Bi_2Sr_2CaCu_2O_{8-\delta}$ (BSCCO). It was shown that this state displays a spontaneous time-reversal symmetry breaking (TRSB). Earlier, Varma [4] predicted the possibility of TRSB in cuprates. They proposed the fascinate ground state with circular microcurrents inside plaquettes of the CuO_2 plane with a definite alignment of the orbital angular momenta associated with these micro-currents. Namely, the up-directed orbital momenta arrange along one diagonal and the down-directed orbital momenta arrange along the other diagonal. The alignment of orbital angular momenta proposed in [4, 5] is not related to any spin alignment.

The aim of the present paper is to discuss an alternative possibility for constructing a state with TRSB. We propose a state in which the TRSB is due to a spiral spin structure. The arguments in favor of this hypothesis are as follows. The electric field of CPL actually interacts only with the orbital motion. Therefore, the TRSB dichroism implies a definite orientation of orbital angular momenta, $\langle L_n \rangle \neq 0$. Such momenta, centered on the atoms, can be induced by aligned spin momenta $\langle S_n \rangle \neq 0$ through the spin–orbit interaction. This implies that a TRSB dichroism D can be observed in ARPES if the photoemission setup can selectively measure the ejected electrons with a definite spin projection $\sigma = \uparrow$ or $\sigma = \downarrow$. The sign of the TRSB dichroism must then depend on the sign of σ. Because the ARPES is usually nonselective with respect to the final spin projection of the ejected electron, the total TRSB dichroism is expected to be zero if the mean spin polarization of the initial states is zero. But for the spiral spin structure, the occupancy $n_{k\sigma}$ of the initial one-electron band state $\{k\sigma\}$ with a definite k depends on σ. Such a spin polarization of the initial k-state can induce nonzero TRSB effects in the ARPES signal. We therefore calculate a dichroism that might manifest in ARPES for the spiral spin configuration of cuprates.

The spiral spin structure has been discussed as a possible ground state of a doped CuO_2 plane. Calculations in the mean field approximation or in the slave boson technique [6–8] were carried out in such a class of functions. The calculations have shown that the spiral state is lower in energy than the antiferromagnet (AF) state and the deviation $\Delta Q = |Q - Q_{AF}|$ of the spirality vector Q from $Q_{AF} = (\pi, \pi)$ increases with doping. The spiral or any other periodic spin structures are associated with incommensurate peaks in the spin susceptibility $\chi(q, \omega)$ as $\omega \to 0$ [9, 10]. Such

*E-mail: movchin@center.chph.ras.ru

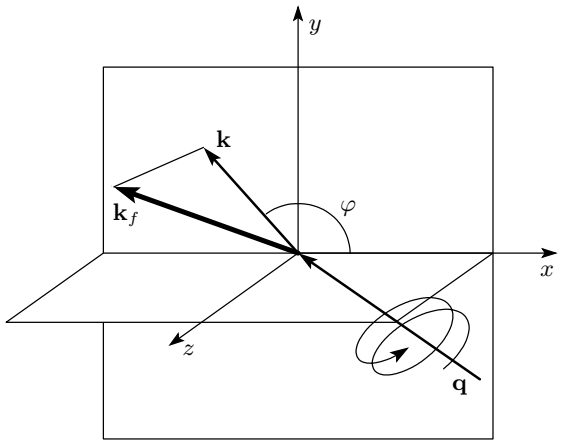

Fig. 1. Setup configuration of the ARPES experiment [3]. The propagation vector $\mathbf{q}_\gamma$ of CPL lies in the mirror plane xz; $\mathbf{k}_f$ and $\mathbf{k}$ are the final momentum of the ejected electron and its component in the CuO_2 plane (xy plane)

peaks have been observed in $La_{1-x}Sr_xCuO_4$ (LSCO) at $q = (\pi \pm \delta, \pi)$, $(\pi, \pi \pm \delta)$ [11]. It is now proved (see [12] and references therein) that the peaks in LSCO are related to the stripe phases. For BSCCO, a variety of hidden orders (spin and charge stripes, orbital AF order, etc.) have been discussed [13, 14]. Latest tunnel spectroscopy studies of BSCCO reveal structures with the periodicity of four unit cells around a vortex or the antiphase AF stripe structure along CuO bonds [15–17]. But the TRSB effect does not display in the static stripe phase. It may be expected in states with the spin or charge currents, such as the spiral spin state. To verify this possibility, we calculate the dichroism of the ARPES signal for the spiral state.

The scheme of the experiment [3] is given in Fig. 1. The right (left) polarized light with a propagation vector $\mathbf{q}_\gamma$ impacts the crystal surface determined by a normal vector $\mathbf{n}$. The xz plane is one of the mirror planes of the crystal with the x axis along the CuO bonds or along the diagonal direction. The ejected electron has a final momentum $\mathbf{k}_f$. The ARPES intensity

$$I \propto |M_{if}|^2 \delta(E_i - E_f - \hbar\omega)$$

is determined by the matrix element of the interaction

$$O = (e/2m_e c)(\mathbf{Ap} + \mathbf{pA})$$

with the field

$$M = A_\alpha F_\alpha, \quad F_\alpha = \langle \psi_f | p_\alpha | \psi_i(k) \rangle \qquad (1)$$

between initial and final states. In the dipole approximation, it contains the vector potential $\mathbf{A}$ of the right ($\zeta_R = 1$) or left ($\zeta_L = -1$) CPL with a complex amplitude,

$$\mathbf{A}_{\mathbf{R(L)}} = A_0[\mathbf{e}_x \cos\theta_\gamma + i\zeta_{R(L)}\mathbf{e}_y + \mathbf{e}_z \sin\theta_\gamma]. \qquad (2)$$

For a given configuration of the setup vectors $\mathbf{n}$, $\mathbf{k}_f$, and $\mathbf{q}_\gamma$, the ARPES dichroism signal D is determined by the relative difference of intensities for the two light polarizations,

$$D = (M_R - M_L)/(M_R + M_L). \qquad (3)$$

We study the symmetry properties of ARPES matrix elements with respect to reflection in the mirror plane of the crystal, which is perpendicular to the surface in a typical photoemission experiment. Following [3], we first consider a time reversal invariant initial state $\psi_i(k)$ and let $\mathbf{q}_\gamma$ and $\mathbf{n}$ lie in the mirror plane m of the crystal (here, the xz plane). The dichroism signal D is then nonzero only if $\mathbf{k}_f$ does not lie in the mirror plane m and D has the opposite signs for k at the different sides of the mirror plane. This dichroism is called geometrical. This large effect has been observed at any doping [3]. But in UD BSCCO, the residual dichroism ($D \neq 0$) has been observed even for a coplanar configuration of $\mathbf{n}$, $\mathbf{k}_f$, and $\mathbf{q}_\gamma$, in which all the three vectors lie in the mirror plane m. In what follows, we let q_z and $\mathbf{q}$ denote the normal and 2D intra-layer components of the photon momentum $\mathbf{q}_\gamma$ and similarly let k_z and $\mathbf{k}$ denote the respective components of the final electron momentum $\mathbf{k}_f$.

We first consider a large geometrical dichroism and then discuss a possible origin of the observed residual dichroism related to TRSB of the ground state of UD cuprate. We suggest that the main contributions to the matrix element are given by space regions inside the atomic spheres. This is in accordance with the fact that frequency dependences of the photoemission intensity roughly repeat the dependences of photoemission cross-sections coming from the corresponding atomic components [18].

The formalism for evaluating the optical matrix element for a general lattice within the KKR scheme is given in [19]. Some corrections must be introduced to provide the common asymptotic behavior $\propto e^{ik_f r}$ of the final wave function of the ejected electron outside the sample ($z > 0$). We restrict our consideration to the one-step model (see [20]) describing the coherent part of photoemission. Generalization to a three-step model requires incorporating rescattering and relaxation processes in order to describe the background in the energy distribution function of the ejected electron. We believe that the one-step model is sufficient for a qualitative description of the angular dependence of dichroism. For

this aim, we use the most simplified form of the initial and final states in the process.

The starting point in calculating F_α in (1) is the KKR wave function for a multicomponent lattice [19]. In the Hartree–Fock representation, the one-particle initial state ψ_i with the quasi-momentum $\mathbf{k}$ is a superposition of orbitals belonging to each center,

$$\psi_i(r,k) = \frac{1}{\sqrt{N}} \sum_{n,\beta} B(n_z) e^{ikr} i^l C^i_{L\beta} \psi^i_{L\beta}(r - R_{n\beta}), \quad (4)$$

where β enumerates all atoms placed at $R_{n\beta}$ in the unit cell $n = (n_x, n_y, n_z)$ and $L = l, m$ are the angular momentum quantum numbers of the orbitals inside each atomic sphere $|r - R_{n\beta}| < a_{n\beta}$. For the upper valence anti-bonding band of the CuO_2 plane, the main orbitals $\psi^i_{L\beta}$ are the $d_{x^2-y^2}$ orbital of Cu and p_x, p_y orbitals of two oxygens O_x, O_y. These orbitals constitute a basis set of the Emery model.

Thus, the initial one-electron state is taken as a superposition of the main real orbitals; in the secondary quantization representation, it is given by

$$\psi_i(k,\sigma) = \sum_{n_z} B_i(n_z) \left[c_d d^\dagger_{k\sigma} + i c_x x^\dagger_{k\sigma} + i c_y y^\dagger_{k\sigma} \right]. \quad (5)$$

The corresponding site operators $d^\dagger_{n\sigma}$, $x^\dagger_{n,\sigma}$, $y^\dagger_{n,\sigma}$ of the Emery model refer to the real functions $d_{x^2-y^2}(r - R_{n,d})$ and $p_\nu(r - R_{n,\nu})$ with $R_{n,\nu} = R_n + e_\nu a/2$, $\nu = x, y$. The functions are considered to extend inside the corresponding atomic (muffin-tin) spheres. The real coefficients c_d, c_x, and c_y in (5) are obtained by solving the Emery model. The summands in Eqs. (4) and (5) refer to a layer number n_z. The amplitudes $B(n_z)$ depending on the distance of the layer from the surface phenomenologically describe a coherent or incoherent interlayer transport along z near the surface depending on the phase correlations between different layers. For the standard bulk initial state ψ_i used in [19], $B(n_z) \propto \exp(ik_z n_z)$.

The final state inside the sample is taken in a similar KKR form with the same in-plane momentum k,

$$\psi_f = \frac{1}{\sqrt{N}} \sum_{n,\beta} B^f(n_z) e^{ikR_{n\beta}} i^l C_{L\beta} Y^*_L \psi_{L\beta}(r - R_{n\beta}). \quad (6)$$

Here, each function $\psi_{L\beta}$ with the angular momentum quantum numbers $L = (l, m)$ is determined inside atomic spheres around the corresponding center $R_{n,\beta}$. The influence of the surface at $z = 0$ is described by introducing the factors $B^f(n_z)$, by phases $\delta_{l,\beta}$ of complex coefficients

$$C_{L\beta} = |C_{L\beta}| e^{\delta_{l\beta}}, \quad (7)$$

and by explicit angular spherical harmonics $Y_L = Y_{lm}(\hat{k}_f)$ depending on the direction of the final momentum k_f. The phases are specific for centers β in the unit cell and for the angular momentum l. These phases arise from matching final state (6) inside the sample with the common plane wave $\propto e^{ik_f r}$ in empty space outside it. The phase modulation of contributions in (6) determines the geometrical dichroism of the photoemission.

The origin of spherical harmonics in Eq. (6) and of the phase modulation of coefficients (7) can be illustrated as follows. We first construct the final state $\psi_{f,\beta}(r)$ for the electron photoemission along the direction $\hat{k}_f$ from one center $\{n, \beta\}$ only. According to [21], it must be a function of continuum with the plane-wave asymptotic form $\propto e^{i\mathbf{k}_f \mathbf{r}}$ and incoming radial waves as $|r - R_{n\beta}| \to \infty$. This final state is

$$\psi_f = \exp(ik_f R_{n\beta}) \times \times \sum_{l,m} i^l e^{i\delta_{l\beta}} Y_{lm}(\hat{r}) Y^*_{lm}(\hat{k}_f) \varphi_l(r_\beta), \quad (8)$$

where $r_\beta = |r - R_{n\beta}|$. The scattering phase $\delta_{l\beta}$ for the orbital momentum l is defined by the asymptotic behavior of the real radial function of continuum,

$$\varphi_{l\beta}(r) \propto \frac{1}{r} \sin\left(kr - \frac{\pi l}{2} + \delta_{l\beta} \right).$$

(According to the KKR approach, we can consider the asymptotic form achieved at the surface of the muffin-tin sphere.)

In a similar manner, the final state ψ_f for the electron ejected from N_s centers of the surface layer must be a function whose asymptotic form at large $z > 0$ is given by a common plane wave $\propto e^{i\mathbf{k}_f \mathbf{r}}$ and incoming spherical waves contributed by different centers.

If $k_f |R_{n\beta} - R_{n'\beta'}| > 1$ and if we neglect the secondary scattering processes, then the final state wave function inside each nonoverlapping muffin-tin sphere surrounding the center $(n\beta)$ of a surface layer must have form (6) with complex coefficients $C_{L'\beta} \propto e^{i\delta_{l\beta}}$. The secondary processes actually synchronize the phases $\delta_{l\beta}$ of all contributions to the final state from different angular harmonics and different centers. The KKR bulk solution for the final state $\psi_f(k_f)$ found in [19] takes the phase and amplitude synchronization of all secondary processes into account, but neglects the necessary additional synchronization and phase modulation coming from the boundary surface where solutions should be matched with the plane wave with momentum k_f.

For a qualitative study of the angular dependence of dichroism and its symmetry, it is sufficient to use the final state in form (6) without specifying the values and phases of $C_{L'\beta}$ in (6). We therefore use Eqs. (5) and (6) for a schematic representation of initial and final states to study the symmetry and possible angular dependence of dichroism manifested in ARPES. The components F_α of matrix element (1) are expressed as a sum of integrals over the interior of atomic spheres with the centers (β) for the corresponding channels $l \to l'$,

$$M_{R(L)} = A_\alpha(\zeta) F_\alpha^\nu(l'\hat{k}). \tag{9}$$

Here, A_α are components of vector potential (2) depending on the right or left polarization of CPL, $\zeta = \zeta_{R(L)} = \pm 1$, and $\hat{k} = \mathbf{k}_f/k_f$. The functions $F_\alpha^\nu(l', \hat{k})$ correspond to real initial orbitals $\nu = d_{x^2-y^2}, p_x, p_y$. To obtain these, we use the selection rules $l' = l \pm 1$ for orbital angular momenta for integrals inside the atomic spheres. For simplicity, we retain only the matrix elements for the transitions $p_{x(y)} \to s, d$ and $d_{x^2-y^2} \to p$ from the $O_{x(y)}$ and Cu centers of the CuO_2 plane. According to the KKR calculations [19], such transitions give the main contributions. Omitting the transition $d_{x^2-y^2} \to f$ at the Cu center does not change the symmetry properties of the calculated dichroism. It leads only to neglecting the small higher harmonics in the angular dependence of the ARPES intensity.

The resulting expressions for the functions $F_\alpha^\nu(l'\hat{k})$ are presented in the Table. For the $p \to s, d$ transitions in oxygen, they also include the factors

$$g_{x(y)} = s_{x(y)}/\sqrt{s_x^2+s_y^2}, \quad s_{x(y)} = \pm \sin(k_{x(y)}/2) \tag{10}$$

that originate from the angular dependence of the real amplitudes $c_{x(y)}$ and c_d of different orbitals in initial band state (5) of the Emery model (with the effective parameters $\epsilon_d, \epsilon_p, t_{pd}, t_{pp}$). At $t_{pp} \ll t_{pd}$, the amplitudes in (5) are

$$c_{x(y)} = g_{x(y)} \sin\eta, \quad c_d = \cos\eta, \tag{11}$$

$$\operatorname{tg} 2\eta = 2t_{pd}(\cos k_x + \cos k_y)/(\epsilon_d - \epsilon_p).$$

Extension to large t_{pp} does not change the symmetry of the amplitudes.

The coefficients $C_{0(\mathrm{I,II})}(k)$ in the Table include 1) the sum over the layers $\sum B_f^*(n_z)B_i(n_z)$ based on the phenomenological or tight-binding dependences $B(n_z)$; 2) the phase factors $\exp(i\delta_{l'})$ coming from boundary conditions; 3) the reduced integrals $\langle l'\beta \parallel p \parallel l\beta\rangle$ over angular variables after removing the m dependence; 4) the radial integrals; 5) the factors $\sin\eta$ and $\cos\eta$ from amplitudes (11).

The functions $F_\alpha^\gamma(l', \hat{k})$ determining the α-components of the matrix element in Eq. (1). The index «γ» enumerates the contributions from different orbitals of the initial state, from $p_{x(y)}$ orbitals of oxygens $O_{x(y)}$ or $d_{x^2-y^2}, d_{xy}$ orbitals of Cu; the final channels s, p, d correspond to the angular momenta $l' = 0, 1, 2$. The respective functions $G_{x(y)}$, L_k, g_x, and g_y, P_k are even and odd functions with respect to the mirror plane zx

$\psi_{i\beta}$	ψ_f	F_x	F_y	F_z
p_x	s	$C_0 g_x$	0	0
p_x	d	$C_\mathrm{I} g_x G_x$	$C_\mathrm{I} g_x P_k$	$C_\mathrm{I} g_x L_k$
p_y	s	0	$C_0 g_y$	0
p_y	d	$C_\mathrm{I} g_y P_k$	$C_\mathrm{I} g_y G_y$	$C_\mathrm{I} g_y L_k$
$d_{x^2-y^2}$	p	$C_\mathrm{II} \sin\theta\cos\varphi$	$-C_\mathrm{II} \sin\theta\sin\varphi$	0
d_{xy}	p	$C_\mathrm{II} \sin\theta\sin\varphi$	$C_\mathrm{II} \sin\theta\cos\varphi$	0

Note: $G_{x(y)} = \pm\sin^2\theta\cos 2\varphi - \cos^2\theta + 1/3$, $g_{x(y)}$ are determined by Eqs. (10), $L_k = \sin 2\theta\cos\varphi$, $P_k = \sin^2\theta\sin 2\varphi$.

The ARPES dichroism signal is then given by

$$D(\varphi) = \mathrm{Im}\{M(\Delta M)^*\}/(|M|^2 + |\Delta M|^2), \tag{12}$$

where $M = M_R + M_L$, $\Delta M = M_R - M_L$, and the angles θ and φ describe the final momentum $\mathbf{k}_f$. Dependence (12) can be represented as $D(\varphi) \propto \tilde{G}(k)\sin\varphi$, where the function $\tilde{G}(k)$ is even with respect to reflection in the mirror plane zx. In accordance with (9), the quantities $M_{R(L)}$ are determined by complex constants C_0, C_I, and C_II, whereas the other angular functions listed in the Table are real. It can be shown that the dichroism signal is zero if all the coefficients $C_{L\beta}$ in (7) have the same phases $\delta_{\beta,l}$ or their differences are multiples of π. A representation of the final state with correct phases is therefore significant for the description of geometrical dichroism.

At $\hat{q}_\gamma = \mathbf{n}$, when the photon impacts normally to the CuO_2 plane, we obtain

$$M = C_\mathrm{II}\sin\theta\cos\varphi + g_x[C_0 - C_\mathrm{I}(\cos^2\theta - \sin^2\theta\cos 2\varphi)] + g_y C_\mathrm{I}\sin^2\theta\sin 2\varphi, \tag{13}$$

$$\Delta M = -C_\mathrm{II}\sin\theta\sin\varphi + g_y[C_0 - C_\mathrm{I}(\cos^2\theta + \sin^2\theta\cos 2\varphi)] + g_x C_\mathrm{I}\sin^2\theta\sin 2\varphi, \tag{14}$$

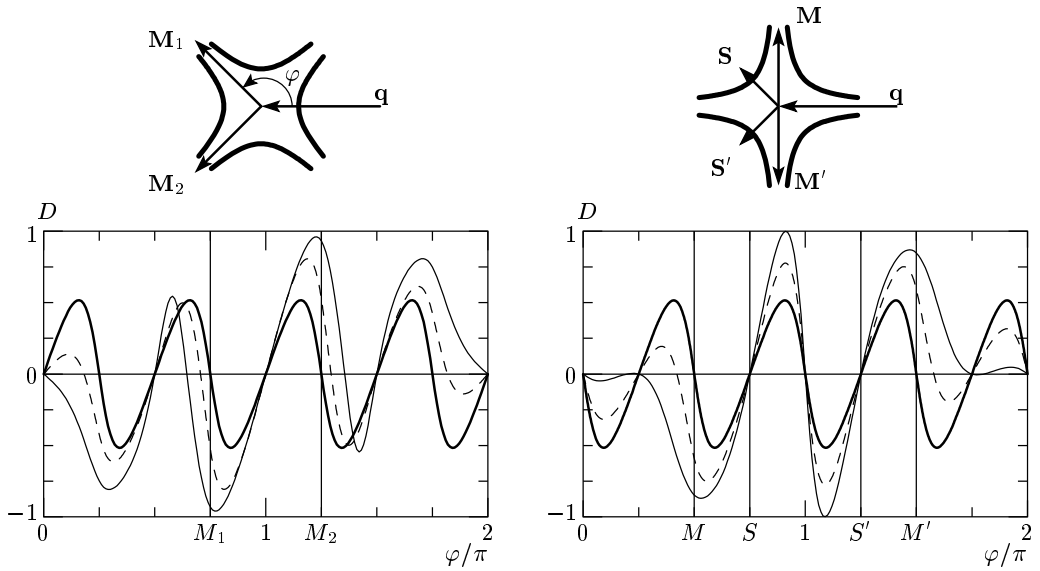

Fig. 2. Dependence of the geometrical dichroism $D(\varphi)$ on the azimuthal angle φ of the vector $\mathbf{k}_f$ for k moving along the nesting lines $|k_x \pm k_y| = \pi$. Solid, dashed, and thin curves correspond to the angles $\theta_\gamma = 0,\ \pi/6,\ \pi/3$ of the photon momentum q. Setup configurations with x along the diagonal direction or along the CuO bonds refer to left or right graphs. Arbitrarily taken coefficients (7) are given in text

where θ and φ are the polar angles of $\mathbf{k}_f$. It follows from (11) and (12) that the dichroism signal is an odd function, $D(-\varphi) = -D(\varphi)$, that vanishes at $\varphi = \pi$ and $\varphi = 0$. This is an expected property of geometrical dichroism.

Manifestations of geometrical dichroism depend on numerous parameters. In Fig. 2, we give examples of the functions $D(\varphi)$ for three angles $\theta_g = 0,\ \pi/6$, and $\pi/3$ of the photon momentum in the mirror plane zx for k moving along the boundary $|k_x \pm k_y| = \pi$ and $k_z = |\mathbf{k} \cdot \mathbf{n}|$. We assign arbitrary values to the relative amplitudes, $|C_0/C_{\rm I}| = |C_0/C_{\rm II}| = 1.0$, and the relative phases $\{\delta_{l'=0}(\mathrm{O}),\ \delta_{l'=2}(\mathrm{O}),\ \delta_{l'=1}(\mathrm{Cu})\} = \{0,\ 3\pi/4, \pi/4\}$ of the coefficients C_0, $C_{\rm I}$, $C_{\rm II}$ in different channels of O and Cu centers. Two setup configurations with x along the CuO bond or along the diagonal direction are considered. The function $D(\varphi)$ is an odd function of φ and vanishes at $\varphi = 0, \pi$. The calculated geometrical dichroism disappears for all φ if all phase differences $\delta_l - \delta_{l'} = \pi m$ are multiples of π. This is the case for the Cu- and O-contributions to the matrix element calculated in [19]. There, the standard KKR bulk wave functions were used and the additional phase modulation was neglected. At the normal photon impact ($\theta_\gamma = 0$), the dichroism signal is zero on each mirror plane of the tetragonal lattice, i.e., at $\varphi = \pi m/4$.

We now take the spin–orbit interaction on Cu into account,

$$V_{LS} = \lambda \sum_n \mathbf{L}_n \mathbf{S}_n, \tag{15}$$

where λ is the corresponding constant. The initial band function $\psi^i_{k\sigma}$ then transforms to $\psi^i_{k\sigma} + \delta\psi$ in a way equivalent to replacement of $d^\dagger_{x^2-y^2,\sigma}$ in (5) by

$$d^\dagger_{x^2-y^2,\sigma} + C_\lambda[2i\xi_\sigma d^\dagger_{xy,\sigma} - \xi_\sigma d^\dagger_{zx,-\sigma} - i d^\dagger_{zy,-\sigma}] \tag{16}$$

in Eqs. (5) and (4). Here, $\xi_\sigma = \sigma/|\sigma| = \pm 1$ and $C_l \propto \lambda/2\delta E$, where δE is the energy difference of the d-orbitals of $x^2 - y^2$ and xy, yz, xz symmetries. The additional contribution to $\psi^i_{k\sigma}$ leads to changes $M \to M + \delta M$, $\Delta M \to \Delta M + \delta\Delta M(\sigma)$ in Eqs. (10), (11), and (12). The TRSB dichroism signal at the normal photon impact ($\theta_\gamma = 0$) is then determined by

$$\delta\Delta M = \xi_\sigma 4 C_\lambda C_{\rm II} \sin\theta \cos\varphi. \tag{17}$$

As a result, the dichroism signal $D(\varphi, \sigma)$ of photoemission with the final momentum k_f and spin projection σ of the ejected electron is given by

$$D(\sigma, k) = A \sin\varphi - \\ - \frac{\xi_\sigma \,\mathrm{Re}(M C^*_{\rm II})}{|M|^2 + |\Delta M|^2} 4 C_\lambda \sin\theta \cos\varphi, \tag{18}$$

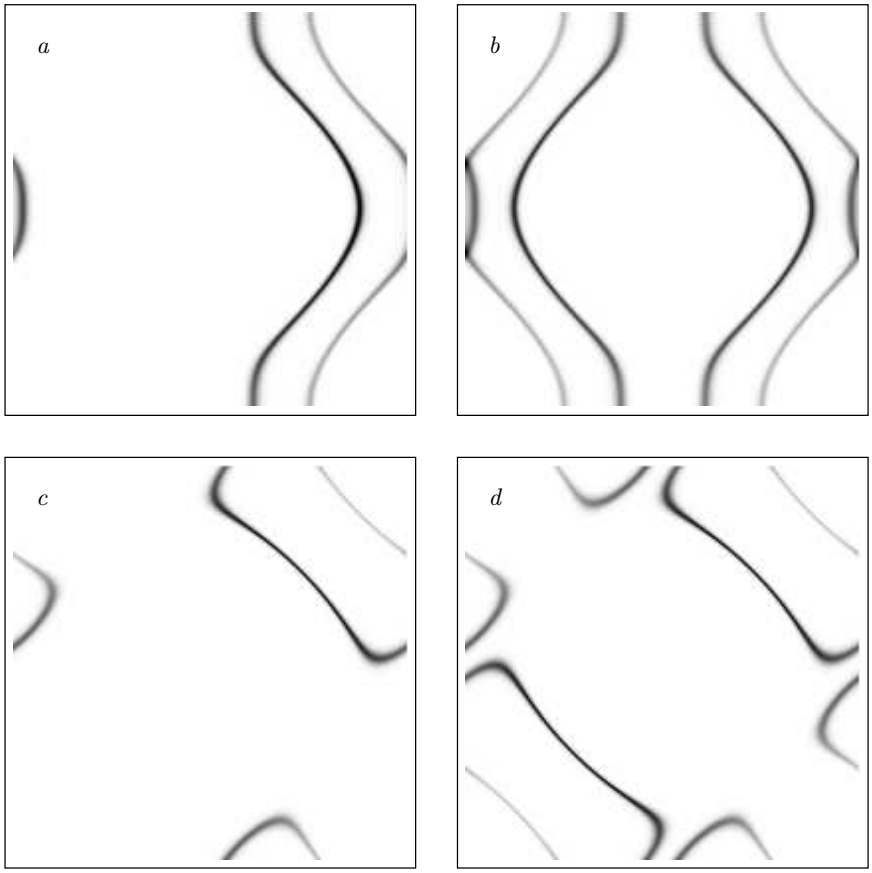

Fig. 3. The images of the spin-selective (plots a, c) and overall (plots b, d) spectral functions $A_\uparrow(k,\omega)$, $A(k,\omega)$ at $\omega = 0$ in the Brillouin zone. The main and shadow Fermi surfaces are shown for the spiral states with the spirality vectors $Q = Q_{\rm I}$ and $Q = Q_{\rm II}$ in (19) (plots a, b and c, d correspondingly)

where M, ΔM, and $C_{\rm II}$ are determined by Eqs. (13), (14), and (7) and by functions in the Table. Only the term that is linear in λ is retained in (18). It is determined only by the admixture of the d_{xy} orbital in Eq. (16). The contributions from d-orbitals of xz, yz symmetries in (16) are of the second order of magnitude in λ. The second term in (18) is an even function of φ and has a nonzero value at $\varphi = 0$ and π when all the three vectors $\mathbf{q}_\gamma$, $\mathbf{n}$, and $\mathbf{k}_f$ lie in the mirror plane xz and geometrical dichroism disappears.

Because the sign of $D(\varphi = 0)$ depends on the sign of the spin projection σ of the ejected electron, the overall dichroism $D = \sum_\sigma D(\sigma, \varphi)$ must be zero for the initial paramagnet (PM) state of the system. For the PM state, the dichroism at $\varphi = 0$ and π can therefore be observed only if the ejected electrons with a definite spin projection on $\mathbf{n}$ are selected. For this PM state, the time reversal symmetry is broken just by a measurement of the spin polarization of the photoelectron.

But there exist TRSB states in which different regions of the k space are characterized by different spin polarizations. For example, for the ground state with a spiral spin structure, the TRSB effect manifests in ARPES by a nonzero overall dichroism at arrangement of all vectors $\mathbf{q}_\gamma, \mathbf{n}, \mathbf{k}_f$ in the mirror plane.

We now demonstrate the polarization selectivity of the level occupancies in the k-space for the spiral state of the 2D $t - t' - U$ Hubbard model. Calculations were carried out for the model with $U/t = 6$, $t'/t = 0.1$ at the doping 0.15 holes per site. The spiral mean-field (MF) solution is characterized by average spins $\langle \mathbf{S}_n \rangle = d(\mathbf{e}_x \cos Qn + \mathbf{e}_y \sin Qn)$ rotating in the xy plane. We study the MF states of two types, with the spirality vectors

$$Q_{\rm I} = (\pi - \delta Q_x, \pi), \quad Q_{\rm II} = (\pi - \delta Q, \pi - \delta Q) \qquad (19)$$

directed along the CuO bond or along the diagonal. The spectral function $A_\sigma(k,\omega)$ at $\omega = 0$ for a definite

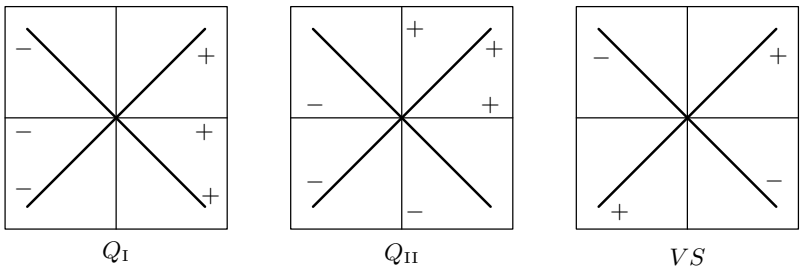

Fig. 4. Relative signs of the TRSB dichroism signal for $\mathbf{k}$ lying on different mirror planes of the lattice for spiral states with the spirality vectors $Q_{\rm I}$ and $Q_{\rm II}$ in (19), or for the state proposed by Varma (VS)

spin projection σ on the z axis (perpendicular to the spin rotation plane) is given by

$$A_\sigma(k,\gamma) = \sum_{i,f} |\langle\psi_f|c_{k\sigma}|\psi_i\rangle|^2 f(E_i)\delta_\Gamma(E_i - E_f), \quad (20)$$

where the Fermi function $f(E_i)$ depends on one-electron levels of the MF solution and $\delta_\Gamma(x)$ is the δ-function broadened with the parameter $\Gamma \sim 0.05t$. In Fig. 3, we show an image of the spin-selective and overall spectral functions $A_{\sigma=\uparrow}(\mathbf{k})$ and $A(\mathbf{k}) = \sum_\sigma A_\sigma$ at $\omega = 0$ for two types of spiral states. Dark and light gray lines in Fig. 3 correspond to the main and shadow spin-selective ($\sigma = \uparrow$) sections of the Fermi surfaces. Similar images for $\sigma = \downarrow$ are obtained from those for $\sigma = \uparrow$ by inversion $\mathbf{k} \to -\mathbf{k}$. The spin dependence of the level occupancy in the k space is related to the spin currents $J_\uparrow = J_\downarrow \propto Q$ existing in the spiral state.

Thus, the TRSB state with a spiral spin structure certainly has spin-selective sections of the Fermi surface. As a consequence, we can observe the TRSB dichroism of the ARPES signal even at a coplanar arrangement of the setup vectors $\mathbf{q}_\gamma, \mathbf{n}$, and $\mathbf{k}_f$ in the mirror plane. Two factors are decisive here. 1) The ARPES signal corresponds to a definite local region of k that is associated with a definite spin polarization for a given spirality vector Q. 2) In accordance with Eqs. (16) and (17), a definite spin polarization induces the orbital angular momenta on Cu centers and corresponding nonzero dichroism at the coplanar setup configuration via the spin–orbit interaction.

In order to estimate the effect, we use the spin–orbit constant $\lambda \sim 800$ cm^{-1} following from the excitation spectrum of Cu^{I}, Cu^{II} [22] and the splitting of d-orbitals $\delta E = E_{x^2-y^2} - E_{xy} \sim 1$–2 eV in the crystal field. We then have the value $C_\lambda = 0.0025$–0.005 for the amplitude in (16). At the setup configuration with $\theta_\gamma = 0$, $\theta = \theta_k = \pi/4$, $\varphi = \pi$ and 0 and with the same arbitrarily chosen coefficients (7) as in Fig. 2 ($|C_{\rm I}/C_0| = |C_{\rm II}/C_0| = 1$, $\delta_{\beta,l} = 0, 3\pi/4, \pi/4$), we obtain for the TRSB dichroism $\max|D| = 0.033$–0.066 at k corresponding $\varphi = 0$ or π lying in the mirror plane. This value is consistent with the TRSB dichroism signal ~ 3–$5\,\%$ observed in UD cuprates [3].

In conclusion, we have shown that the TRSB dichroism observed in the ARPES spectra of the UD cuprates may be related to a local spiral spin order in the system. This hypothesis differs from the model TRSB state proposed by Varma et al. [4, 5], who connect the TRSB with aligned charge circular microcurrents on plaquettes of the CuO_2 plane. Instead, the spiral spin order implies the appearance of local spin currents $\mathbf{J}_\uparrow = -\mathbf{J}_\downarrow$ of a macro scale, about the domain size. The existence of different domains with different signs and values of the TRSB dichroism signal has been shown by studying a set of samples of UD BSCCO in [3]. The following test for the new hypothesis may be proposed. The rotation of the sample by 180° around the z axis does change the sign of the TRSB dichroism $D(\varphi = \pi)$ in our hypothesis and does not change the sign in case of the TRSB state constructed in [4]. In the former case, the rotation changes the signs of the spin currents and of the spin polarization. Relative signs of the TRSB dichroism signal at different mirror planes of cuprate for two types of spiral states (19) and for the state proposed by Varma are illustrated in Fig. 4. These signs can be measured only if the ARPES signal comes from the same domain of a sample before and after its rotation and if the spin currents of the spiral state are pinned during the rotation of the sample. We note that for the ferromagnet alignment of spins in surface layers, the TRSB dichroism has the same signs along all directions in mirror planes of the lattice.

Great sensitivity of the Fermi surface (FS) to the spin structure leads to the questions that are important for understanding the pseudogap state of BSCCO: is the observed FS a composed result coming

from several domains with different currents? What is the dynamics of these currents and domains in the UD cuprates? Can the spin fluctuations be frozen near the surface into static domains with a spiral or ferromagnet spin order? We note that the ARPES technique probes only a few surface layers. Observing the TRSB effect with the use of ARPES therefore requires a correlated spiral order only in these few surface layers, whereas the bulk TRSB effect may be destroyed. An additional test for the supposed local spiral order is possible. One can measure the spin polarization $\langle \mathbf{S} \rangle$ of electrons ejected from different sections of the Fermi surface and check the correlations of the direction of $\langle \mathbf{S} \rangle$ with the sign of the TRSB dichroism signal $D(\varphi)$ at $\varphi = \pi$. This program requires a spin-selective detection of photoelectrons. Such detection is now realized in a total «spin–orbit photoemission» measurement [23]. Its application in ARPES might elucidate the nature of TRSB dichroism of photoemission from UD cuprate.

This work is supported by the RFBR (grants № 00-03-32981 and № 00-15-97334). The author is grateful to A. A. Ovchinnikov and V. Ya. Krivnov for useful discussions.

REFERENCES

1. T. Timusk and B. Statt, Rep. Progr. Phys. **62**, 61 (1999).
2. J. C. Campusano, M. R. Norman, and M. Raderia, in *Physics of Conventional and Unconventional Superconductors*, ed. by K. H. Benneman, J. B. Ketterson, E-print archives, cond-mat/0209476.
3. A. Kaminsky, S. Rosenkranz, H. M. Fretwell, J. C. Campuzano, Z. Li, H. Raffy, W. G. Cullen, H. You, C. G. Olson, C. M. Varma, and H. Höchst, E-print archives, cond-mat/0203133.
4. C. M. Varma, Phys. Rev. B **61**, R3804 (2000).
5. M. E. Simon and C. M. Varma, E-print archives, cond-mat/0201036.
6. B. I. Shramian and E. D. Siggia, Phys. Rev. B **40**, 9162 (1989).
7. R. Fresard and P. Woelfle, J. Phys.: Condens. Matter **4**, 3625 (1992).
8. P. J. M. Denteneer and H. Blaubaer, J. Phys.: Condens. Matter **7**, 115 (1995).
9. A. V. Chubukov and K. A. Musaelyan, Phys. Rev. B **51**, 12605 (1995); J. Phys.: Condens. Matter. **7**, L153 (1995).
10. K. Krüger and S. Scheidl, E-print archives, cond-mat/0211593.
11. Ph. Bourges, in *The Gap Symmetry and Fluctuations in High Temperature Superconductors*, ed. by J. Bok, G. Deutscher, D. Pavuna, and S. A. Wolf, Plenum Press (1998).
12. B. Khaykovich, R. J. Birgeneau, F. C. Chou et al., E-print archives, cond-mat/0209648.
13. S. A. Kivelson, E. Fradkin, J. M. Tranquada et al., E-print archives, cond-mat/0210683.
14. S. Sachdev, E-print archives, cond-mat/0211005, cond-mat/0203363, A. Polkovnikov, M. Vojta, and S. Sachdev, Phys. Rev. B **65**, 220509 (2002); S. Sachdev and S. C. Zhang, Science B **295**, 452 (2002).
15. B. Lake, G. Aeppli, K. N. Clausen et al., Science **291**, 1759 (2001).
16. J. E. Hoffman, E. V. Hudson, K. M. Lang et al., Science **295**, 466 (2002).
17. C. Howald, H. Eisaki, N. Kaneko, and A. Kapitulnik, E-print archives, cond-mat/0201546.
18. Y. Sakisaka, J. Electr. Spectr. Relat. Phenom. **66**, 387 (1994).
19. M. Lindroos, S. Sahrakorpi, and A. Bansil, E-print archives, cond-mat/0109039, Phys. Rev. B **65**, 054514 (2002).
20. A. Damascelli, Z. X. Shen, and Z. Hussain, E-print archives, cond-mat/0208504.
21. L. D. Landau and E. M. Lifshitz, *Quantum Mechanics*, Nauka, Moskva (1989).
22. *Atomic Energy Levels*, ed. R. F. Bacher, S. Goudsmoth, McGraw-Hill Book Company, New York–London (1932).
23. G. Ghiringhelli, L. H. Tjeng, A. Tanaka et al., Phys. Rev. B **66**, 75101 (2002).